Dielectric Response of Electron-doped Ionic Superconductor Li_xZrNCl

Antia S. Botana[1] and Warren E. Pickett[1]

[1]*Department of Physics, University of California, Davis, CA 95616, USA*

(Dated: August 18, 2014)

When electron doped, the layered transition metal nitrides $\mathcal{T}$NCl ($\mathcal{T}$ = group IVB transition metal ion) become impressive superconductors with critical temperature T_c= 15-26K. Here we take the most studied member, ZrNCl, as a representative and calculate the dielectric response $\epsilon(\omega)$ versus frequency and concentration of doped electronic carriers. The static dielectric constant ϵ_∞=5 is reproduced extremely well. We establish that the differences between rigid band modeling and virtual crystal treatment are small, and compare also with actual lithium doping using supercells. We obtain the variations upon changing the doping level of the reflectivity and energy loss function as well, many of which are found not to be correlated with the observed (non)variation of $T_c(x)$. The main plasmon peaks appear where the electron gas model suggests, in the range 1.2-2.0 eV for x varying from 0.16 to 0.50.

PACS numbers: 74.25.Gz, 77.22.-d, 31.15.E-

I. INTRODUCTION AND BACKGROUND

Superconductivity in doped quasi-two-dimensional compounds or at surfaces has been a focus of interest of the community since the work of Ginzburg,[1,2] and has gained fevered activity after the discovery of the strong dependence of the critical temperature (T_c) upon intercalation of the transition metal dichalcogenides and the discovery of high T_c in 2D cuprates. The way in which doping of 2D layers modifies the electronic behavior of a compound giving rise to superconductivity greatly depends on the specific system. In copper oxides there is a magnetic insulator to strange metal transition that completely modifies the electronic structure. However, in bismuthates and in electron-doped nitridochloride $A_x\mathcal{T}$NCl superconductors (where $\mathcal{T}$ is a group IVB transition metal Ti, Zr, Hf) there is only Pauli paramagnetic behavior. The cause of superconductivity in this latter class of materials remains unknown, with neither spin nor conventional phonons being responsible for their superconducting behavior, as we discuss below.[3]

The superconductivity in transition metal nitridochlorides (with maximum T_c = 17, 15, 26 K for Ti, Zr, Hf respectively) emerges when the insulating parent compounds are electron-doped.[4–6] To clarify the mechanism of superconductivity an understanding of the electronic behavior is crucial because only then can the key issue of electron pairing be addressed. Electron doping in the metal nitride double honeycomb planes, as shown in Fig. 1, is achieved by intercalation of alkali ions into the van der Waals gap between Cl layers. Large organic molecules may also be included.[7–9] However, the origin of the high T_c remains unknown, as the characteristics of this class of superconductors are unique. There is a low DOS at the Fermi level and a weak electron phonon coupling has been suggested both experimentally[10,11] and theoretically.[12,13]

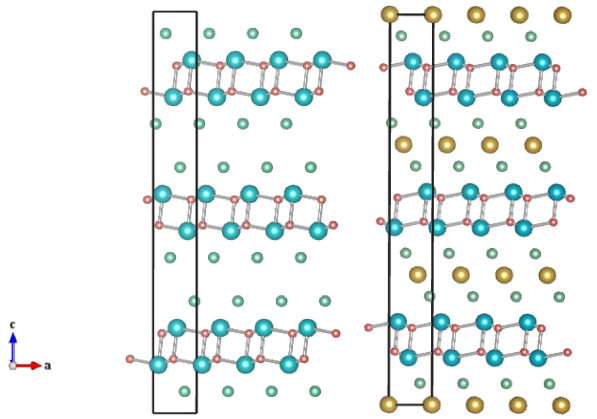

FIG. 1: Crystal structure of ZrNCl (left) and the doped compound $Li_{0.5}$ZrNCl (right). Zr atoms are blue, N red, Cl green and Li yellow.

There are several unusual characteristics that make the $A_x\mathcal{T}$NCl class of superconductors unique. First, and an aspect that is not usually emphasized, they are extremely bad conductors, with reported residual resistivity (T→0) of $10^3 - 10^5$ $\mu\Omega$ cm.[4,7–9,14] In some cases the temperature dependence crosses from metallic to semiconducting and weak localization behavior arises just above T_c. Second, except near the critical concentration x_{cr} where the insulator to metal transition occurs,[10] T_c is almost independent of the doping level x whereas the Fermi level DOS undergoes a change as doping is increased. Specifically, there is no superconducting dome, and the constancy of T_c continues well into the region where the density of states at the calculated Fermi level $N(E_F)$ increases sharply, as the $\mathcal{T}$ ion d states

other than the in-plane $d_{xy}, d_{x^2-y^2}$ orbitals begin to be filled.[15] Thirdly, there is one property that correlates strongly with T_c: the separation of the $\mathcal{T}N$ bilayers along the z direction. For the Hf and Zr counterparts, from the minimum separation, at small Li intercalation, T_c increases sharply by ≈30% before leveling off and remaining nearly constant up to the largest separations that have been achieved ($\sim$ 20 Å), by introducing large molecules along with the dopant metal atoms.[7,8] Thus the superconductivity in these systems is truly 2D.

The very "bad conductor" aspect can be clarified by trying to apply conventional Fermi liquid metallic formalism. Interpreting the residual resistivity $\rho_\circ = 4\pi/\Omega_p^2\tau \sim 10^4$ $\mu\Omega$ cm gives, with in-plane $\hbar\Omega_p \approx 3$ eV, $\hbar/\tau \sim 10$ eV, corresponding to a totally washed out band structure. Putting τ together with the Fermi velocity $v_F \approx 10^8$ cm/s leads to a mean free path ($l = 2\pi/\Delta k$) that implies the Brillouin zone (BZ) would be completely wiped out. This analysis indicates the transport is not metallic, and an alternative picture is needed to understand electronic behavior.

Takano *et al.*, on the other hand, use the measured superconducting coherence length ξ, the BCS relation for ξ_0, and the phenomenological relation $\xi^{-1} = \xi_0^{-1} + l^{-1}$ to infer values of $l\sim$ 10 nm for their samples.[14] In any case, the lack of consistency in these interpretations indicates problems with Fermi liquid theory for transport. This conclusion gains support from the recent report from ^{91}Zr and ^{15}N NMR studies[16], which finds pseudogap character typical of non-Fermi liquid phases in the $0.06 \leq x \leq 0.10$ regime. This is the regime where enhanced susceptibility is reported;[17] curiously, the NMR data show no evidence of enhanced spin fluctuations on the verge of the superconductor to insulator transition, causing difficulties for applying a model of pairing by this mechanism. Kuroki proposed that the high T_c in doped Hf/ZrNCl is a characteristic feature of the spin fluctuation-mediated superconductivity in a honeycomb lattice.[18]

Superconductivity emerges in this system from a very badly conducting state. Jaramillo *et al.*[19] have proposed that a strong interaction that can shift spectral weight over a large energy scale is necessary for bad metal conductivity. In the case of rare-earth nickelates, this strong interaction happens between lattice distortions and Ni-O covalence, but its origin may vary depending on the system (and nickelates do not superconduct). The question of whether this explanation may apply to the bad conductivity in $A_x\mathcal{T}$NCl superconductors and if so, what the driving interaction might be, is still open.

There is no local moment behavior, so the electronic state and the pairing mechanism are very different from the high temperature superconducting cuprates and Fe-based materials. Based on the standard Landau Fermi liquid (metallic) viewpoint, the electron-phonon coupling has been calculated to be clearly too weak to account for the observed values of T_c.[12,13] From density functional theory (DFT) based calculations for Li-doped ZrNCl, T_c of only 5 K is obtained, using a typical value of the Coulomb pseudopotential for a normal metal $\mu^* = 0.1$.[12] A suggestion was made by Yin *et al.*[20] that a different exchange-correlation functional, the hybrid (part unscreened exchange) functional, is more appropriate for this class of doped insulators. They found that the additional exchange potential increases the shifts of certain bands due to selected frozen phonon modes, giving them an enhanced electron-phonon coupling. However, a full calculation was not carried out. In any case, whichever functional is chosen, it seems apparent from the observed resistivity that Li_xZrNCl has no transport Fermi surface at all, or very few mobile carriers, or both.

The N isotope shift of T_c seems to be non-zero but is so small as to be very discouraging for any lattice mechanism relying on N displacements.[21,22] The density functional theory for superconductors (SCDFT)[23] has been shown to reproduce the observed T_c of a selection of phonon-mediated superconductors.[24–26] This approach differs largely in the DFT-based treatment of the Coulomb interaction. When SCDFT was applied to $\mathcal{T}$NCl superconductors,[15] a T_c of only 4.3 K and 10.5 K was obtained for the Zr and Hf counterparts, respectively. In addition, T_c increases with increasing doping level in clear contrast to the experimental results. In Li_xZrNCl, an enhancement of T_c with a reduction in the carrier density in the low doping regime towards the metal-insulator transition has been observed.[10]

Several works have tried to consider the origin of pairing in strongly layered superconductors beyond the standard Migdal-Eliashberg ansatz. Bill *et al.*[27,28] have considered that the dynamical screening of the Coulomb interaction is essentially different in layered structures, and built a model that provides for an additional contribution to the pairing from dynamical electronic screening and low energy plasmons, which leads to a drastic enhancement of T_c in $\mathcal{T}$NCl superconductors. We also mention the work of Pashitskii and Pentegov[29] that has included classes of vertex corrections within the picture of a plasmon mechanism of pairing.

To elucidate the electronic behavior and help to understand the origin of the unique properties of this class, we analyze the dependence of the dielectric response on frequency and concentration for Li_xZrNCl calculated within the random phase approximation

from the Kohn Sham band structure. This treatment is consistent with the Landau Fermi liquid picture which as we have noted is quite suspect for transport but may yet apply for higher energy excitations.

The paper is organized as follows. After describing the computational methods and crystal structure in Sections II and III, we revisit the electronic structure of the pristine compound and Li_xZrNCl ($x = 0.16$, 0.25 and 0.50), analyzed using supercells to reproduce the desired doping levels (Section IV). The obtained electronic structure of the doped compounds is then contrasted to that obtained using the virtual crystal approximation (VCA). In Section V, the dielectric response versus frequency and concentration is discussed. Differences in the dielectric behavior do not correlate with doping in the observed variation of $T_c(x)$ suggesting that pairing based on the electronic overscreening is not a viable picture.

II. STRUCTURE

Although the compound β-ZrNCl has been known since the 60's, its crystal structure was for some time under debate.[30–32] We have used the structures determined by x-ray diffraction on single crystals[31] that confirmed the results obtained by others using neutron powder diffraction.[33]

The structure of the insulating parent compound β-ZrNCl is shown in the left panel of Fig. 1. The central structural units are double honeycomb layers of ZrN sandwiched between two Cl layers leading to a neutral ZrNCl unit. Adjacent ZrN layers are rotated such that a short Zr-N interlayer bond exists. Each Zr atom is bonded to four neighboring N, three belonging to the same ZrN layer and one to the adjacent layer. The bonding between the ZrNCl units is of a weak van der Waals type, allowing intercalation by alkali ions and also by large organic molecules. Neighboring $Zr_2N_3Cl_2$ slabs are shifted relative to each other, resulting in a rhombohedral space group $R\bar{3}M$.

Upon Li doping, the dopants occupy a high symmetry site ($3a$) within the van der Waals gap between two Cl layers (see right panel of Fig. 1). As there is one such $3a$ site per bilayer, full occupancy corresponds to a doping level of x =0.5. The space group is not changed but the shift between neighboring bilayers is altered in such a manner that the stacking sequence is changed from ABC to ACB upon Li intercalation (see Fig. 1).

III. COMPUTATIONAL METHODS

T_c does not change for the range $x = 0.16$ to 0.50 so this is the doping range we will focus on, performing calculations for $x = 0.16$, 0.25 and 0.5.[17] The different doping levels have been achieved in two different ways: (i) constructing supercells from the structural data for $Li_{0.21}ZrNCl$ (full occupancy of the $3a$ site) introducing Li vacancies to reach the desired doping level (for $x = 0.16$, $3 \times 2 \times 1$, for x= 0.25, $2 \times 2 \times 1$), (ii) using virtual crystal approximation (VCA) to avoid the use of supercells. In this case an artificial doping is achieved changing the electron count to the desired level to account for a certain doping. A doping level of 0.16 would correspond to 1/3 occupation of the Li site and 0.25 to 1/2. Two models can be used: without Li, but with 1/2(1/3) electrons per unit cell added to simulate the Li doping of 0.25(0.16) starting from the structure of ZrNCl or with one Li per unit cell (full occupancy) but removing 2/3(1/2) electrons to reach the same doping levels of 0.16(0.25).[12]

The electronic structure calculations were performed with the WIEN2k code,[34,35] based on density functional theory[36,37] (DFT) utilizing the augmented plane wave plus local orbitals method (APW+lo).[38] All structures were fully relaxed using the generalized gradient approximation (GGA) PBE scheme[39] and the lattice parameters were optimized within the same scheme. The lattice parameters used in the calculations for the doped compound were $a = 3.60$ Å and $c = 27.83$ Å; for the undoped compound, $a = 3.59$ Å and $c = 27.67$ Å.

The calculations were well converged with respect to the k-mesh and $R_{mt}K_{max}$. $R_{mt}K_{max}$= 7.0 was chosen for all the calculations. Selected muffin tin radii were the following: 2.07 a.u. for Li, 2.42 for Cl, 2.00 for Zr and 1.72 a.u. for N.

The optical properties were obtained using the optic code implemented within WIEN2k. The theoretical background is described in detail in Ref. 40. The calculation of optical properties requires a dense mesh of eigenvalues and the corresponding eigenvectors (up to 10000 k points were used for Li_xZrNCl).

The program optic generates the symmetrized squared momentum matrix elements between all band combinations for each k-point, then it carries out the BZ integration. The interband and the intraband contributions to the imaginary part of the dielectric tensor are discussed separately in Section V. The Kramers-Kronig transform real component can be computed allowing the evaluation of the optical conductivity, loss function, and reflectivity.[40]

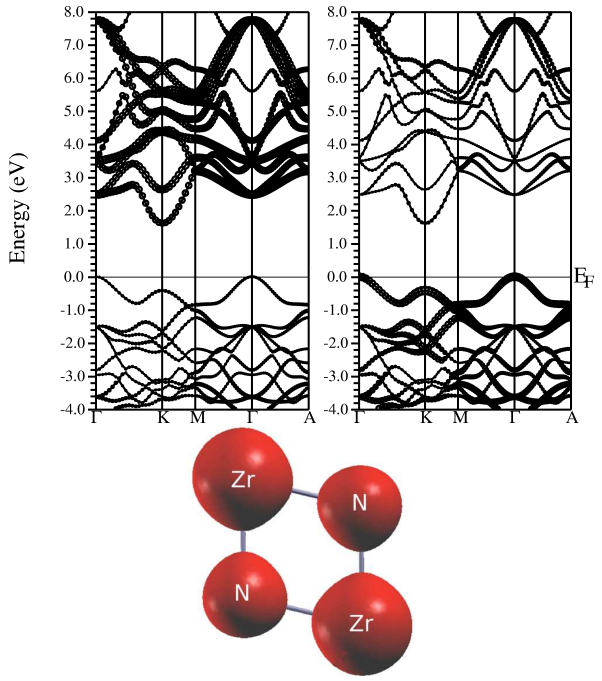

FIG. 2: Top panels. Band structure along high symmetry direction with band character emphasized, for ZrNCl. Left Zr 3d, right N 2p character, is highlighted. The size of the symbols is proportional to the Zr or N character of the corresponding eigenfunction. Bottom panel: three dimensional isocontour plot of the charge density for the ZrN bilayer obtained using the Xcrysden package.[41] The nearly spherical density obtained for both Zr and N atoms reflects that substantial Zr 3d character is mixed into the occupied N 2p bands, somewhat reducing the ionic character from nominal values.

IV. ELECTRONIC STRUCTURE, WITH ZRNCL AS THE PROTOTYPE

A. Undoped ZrNCl

The electronic structure of ZrNCl, with filled N 2p and Cl 2p bands and empty Zr 3d bands, is well characterized by the formal ionic description $Zr^{4+}N^{3-}Cl^{1-}$. Zr-N covalency is however substantial, so ZrNCl is quite different from a purely ionic insulator. In Fig. 2 the band structure with band character plot for Zr and N atoms is shown. The band gap value for the parent compound determined experimentally is 2.5 eV,[42] the one derived within GGA is 1.7 eV. The conduction band is dominated by empty Zr-d states above the gap. The k_z dispersion along $\Gamma - A$ in the undoped compound, which is comparable to in-plane dispersion, is due to the small interlayer distance. This dispersion will disappear when Li is placed between the $(ZrNCl)_2$ slabs, thereby separating the layers and practically eliminating overlap between them.

The Cl and N states are mixed in the valence band region, though at the top of the valence band N states dominate. The lowest lying conduction bands (at K) are formed precisely from the Zr d_{xy}, $d_{x^2-y^2}$ orbitals, and the bands just below the gap are N p_x, p_y states.[43] With 3-fold in-plane coordination, N p_x, p_y orbitals should be thought analogously to the sp^2 orbitals in graphene. Likewise, the Zr d orbitals should be pictured in terms of 3-fold symmetry adapted orbitals, for both pairs ($d_{x^2-y^2}$,d_{xy}) and (d_{xz}, d_{yz}). However, isovalent TiNCl with T_c=17 K has an orthorhombic structure,[44] so it seems clear that the honeycomb structure of ZrNCl and HfNCl does not play a specific role in the occurrence of high temperature superconductivity in this materials class.

The electron carriers go into states largely on Zr, with lobes of maximum charge pointing *between* neighboring N ions, as the crystal field picture would suggest. The density on the N ions, according to the same picture is oriented directly at the positive Zr ions. The Zr-N hybridization is best characterized as antibonding.[13] The d_{xz},d_{yz} and d_{z^2} orbitals lie successively higher in energy.

B. Li_xZrNCl supercells

The band structures for Li_xZrNCl x= 0.16, 0.25 (using supercells) and x= 0.50 are shown in Fig. 3. Neither the structural changes nor the occupation of the Li site seem to alter significantly the shape of the lowest conduction band except to greatly decrease k_z dispersion due to separation of the constituent layers. The differences that are visible can be ascribed to supercell effects arising from the (artificial) periodicity.

The densities of states (DOS) for the various doping levels are shown in Fig. 4 with the zero of energy set at the bottom of the conduction band. The lowest band is characterized by a small density of states at the Fermi level and a small effective mass as shown in Fig. 4 ($N(E_F)$= 0.34 states/eV f.u corresponds to an effective mass m^*=0.66 m).[12] The Fermi level (dashed lines) for the two lowest doping levels (x= 0.16 and 0.25) lies within this band with low DOS. For x = 0.5, states other than the lowest in-plane $d_{x^2-y^2}$+d_{xy} begin to be filled with correspondingly higher N(E_F). The valence bandwidths reported experimentally are 6.1 for the parent compound and 7.0 for $Li_{0.25}$ZrNCl,[42] underestimated (which is not uncommon) by calculations performed using GGA. The DOS gives a clearer view of the fact that, upon electron doping, except for a shift in the chemical potential, the change in position of

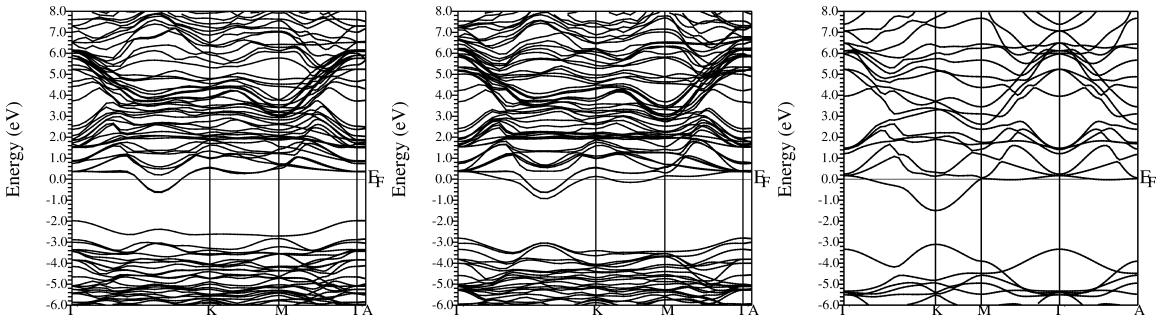

FIG. 3: Band structure of Li_xZrNCl. From left to right x= 0.16, 0.25 (supercells) and 0.50 (not supercell).

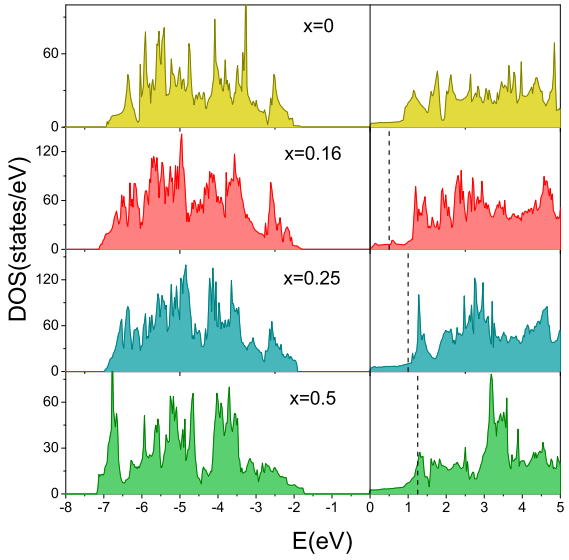

FIG. 4: Total DOS for ZrNCl and Li_xZrNCl with increasing x (from top to bottom). The zero energy is set at the bottom of the conduction band. The Fermi level is marked with a dashed line. Note that the DOS at the top of the valence band changes, i.e. it is not rigid band like.

E_F for higher doping levels, and some changes in the first peak in the DOS appearing at about 1 eV above the bottom of the conduction band, it remains unchanged. In the valence band region, bigger changes take place, the DOS at the top of the valence band changes not being only a rigid-band like shift. This difference should be irrelevant to superconductivity though.

The specific heat (C_v) jump at T_c is a measure of N(0) (and the density of pairs that are formed). The observed extremely bad metallic character suggests that only a very small density of pairs may be formed at T_c. In BCS or Eliashberg-type materials, ΔC_v = 2-3 γT_c, where γ is the specific heat γ proportional to N(0) $\gamma = 2/3(1+\lambda)\pi^2 k_B^2 N(0)$. From the experimentally determined γ= 1.1 mJ/molK^2 using $N(0) = 0.19 - 0.26$ states/(eV spin f.u) a $\lambda \leq 0.22$ has been obtained by Iwasa *et al.*[11,45] This value belongs to the weak coupling regime and will never produce any finite value of T_c once the Coulomb pseudopotential μ^*= 0.10-0.15 is included.

C. Li_xZrNCl within VCA

Given the impressive superconductivity in this system and the uncertain nature of the pairing mechanism, it is important to quantify the effect on the electronic structure of including Li explicitly, and on the method of doing so. This aspect of charge rearrangement due to doping was found to be surprisingly large[46] in (Al,Mg)CuO_2, another layered transition metal compound. We have evaluated the electronic structure of Li_xZrNCl within VCA using two alternative strategies: removing electrons from the stoichiometric structure of $Li_{0.5}ZrNCl$ (one f.u. is $Li(ZrNCl)_2$) and adding electrons from ZrNCl.[12] We find that actual occupation of the Li site does not alter the band structure in any significant way, with carrier doping occurring in a rigid band fashion as has been assumed in all previous works both theoretical (band structure calculations)[12] and experimental (optical reflectivity measurements).[47] For the lowest doping levels studied electrons will fill only the same single band with minimum at K with Zr-($d_{x^2-y^2}$,d_{xy}) character using both VCA methods. For x= 0.5, some out of plane d-states start being occupied as shown in the previous section. In Na-doped ZrNCl and HfNCl, photoemission spectroscopy studies[48,49] have shown non-rigid like behavior against theoretical predictions.[13] The behavior appears as spectral weight shifts, whereas peak centroids remain rigid-band like.

The similarity of the electronic structures in the

vicinity of the Fermi energy for empty and full occupation of the Li shows that, as far as the electronic properties are concerned, the Li atoms simply act as donators of electrons to the ZrN bilayers, which can justify a simpler doping study using VCA instead of the more computationally demanding use of supercells.

D. Electron density plots for Li_xZrNCl

In Fig. 5 we show a three dimensional (3D) isocontour plot of the doped electron density for each non zero value of k (from only the conduction bands) as well as a contour plot in a plane lying within one ZrN layer. The density at small doping was earlier characterized as Zr $d_{x^2-y^2}$, d_{xy} and N p_x, p_y character.[13] For $x = 0.16$ and 0.25, the 3D plot demonstrates that this characterization is incomplete, because the lobes on Zr lie alternately above and below its equatorial plane. Thus there is significant d_{xz}, d_{yz} mixture due to structural asymmetries. The contour plots confirm that the maxima around the Zr atoms are oriented between, rather than towards, the nearby N anions, a simple crystal field effect.

For $x = 0.5$ new bands contribute to the density (see Fig. 4) which is reflected in a dramatic reorientation of the high density lobes being directed towards N, with formation of a more bonding-like structure between Zr and N. This substantial change is not reflected in superconducting behavior however, as T_c is observed to depend hardly at all on the doping level in the range we have considered.[7]

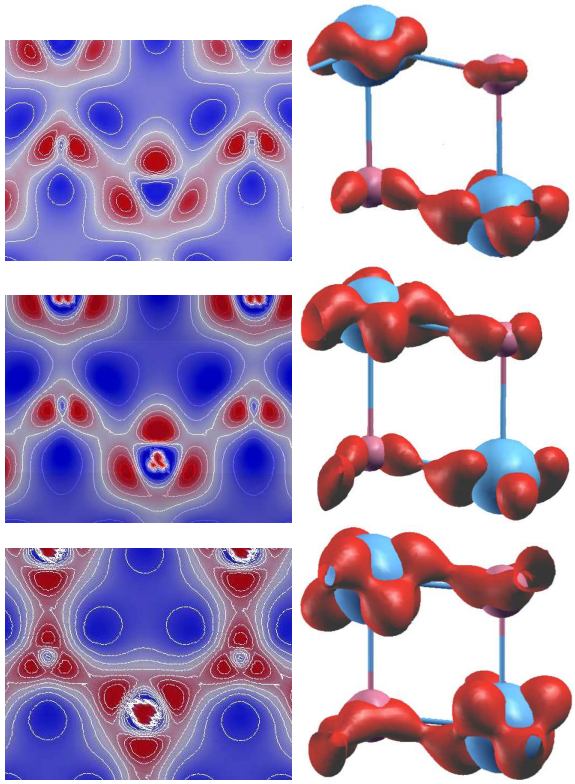

FIG. 5: Left panels: contour plots for Li_xZrNCl for increasing values of $x = 0.16, 0.25$ and 0.50 from top to bottom. The plane of the figure lies between Zr and N layers, which are only roughly coplanar. Right panels: the corresponding three dimensional isocontour plot of the electron density obtained using Xcrysden.[41] The blue and pink spheres represent Zr and N respectively.

V. DIELECTRIC RESPONSE OF LI_xZRNCL

For the symmetry of Li_xZrNCl the dielectric tensor is diagonal with only in-plane xx and perpendicular zz components. For simplicity, and because electronic structure differences between supercell and VCA calculations are small, we present calculations using VCA and the primitive cell to evaluate the imaginary part of the q=0 dielectric tensor within the random phase approximation (RPA). The calculation takes the usual expression requiring the band energies and momentum matrix elements between Kohn-Sham wavefunctions.[40,50,51] For x$\geq$ 0, we focus on the results obtained from VCA calculations in which electrons are removed from $Li_{0.5}ZrNCl$.

We have performed calculations for the polarization parallel to the ZrN planes and also for the perpendicular polarization to study anisotropy and discriminate the contribution of the ZrN planes making possible to identify the excitations in the ZrN plane and to further characterize the electronic structure of that plane for the respective doping level.

A. Handling of the Intraband Part

Without considering scattering, the intraband part is a δ-function at ω=0 with strength given by the Drude plasma frequency Ω_p obtained from the Fermi surface average density of states and velocity $\vec{v}_k$ averages

$$\Omega^2_{p,\alpha\alpha} = 4\pi e^2 N(0) v^2_{F,\alpha}. \quad (1)$$

Considering that electrons are always interacting, with electrons, with phonons, and with defects, a lifetime broadening γ is introduced, leading to the form

$$\epsilon^{intra}_{2,\alpha\alpha}(\omega) = \frac{\gamma \Omega^2_{p,\alpha\alpha}}{\omega(\omega^2 + \gamma^2)} \quad (2)$$

with Kramers-Kronig transform

$$\epsilon^{intra}_{1,\alpha\alpha}(\omega) = 1 - \frac{\Omega^2_{p,\alpha\alpha}}{\omega^2+\gamma^2} \quad (3)$$

from the combined expression

$$\epsilon^{intra}_{\alpha\alpha}(\omega) = 1 - \frac{\Omega^2_{p,\alpha\alpha}}{\omega^2+\gamma^2}(1 - i\frac{\gamma}{\omega}) = 1 - \frac{\Omega^2_{p,\alpha\alpha}}{\omega(\omega+i\gamma)}.$$

The imaginary part retains the $\omega \to 0$ divergence of a metal. Given no relevant experimental information, we have used $\gamma = 0.1$ eV throughout, corresponding to a relaxation time $\tau \approx 7\times 10^{-15}$ s.

The calculated plasma frequencies in eV for the x= 0.21 structure (interlayer distance= 9.28 Å) are

$$\begin{aligned} x = 0.16 \quad & \Omega_{p,xx} = 2.97, \quad & \Omega_{pl,zz} = 0.70 \\ x = 0.25 \quad & \Omega_{p,xx} = 3.14, \quad & \Omega_{pl,zz} = 0.68 \\ x = 0.50 \quad & \Omega_{p,xx} = 2.80, \quad & \Omega_{pl,zz} = 0.71 \end{aligned} \quad (4)$$

The first two values of $\Omega_{p,xx}$ are roughly consistent with a constant DOS with initial doping and $v_F \propto k_F \propto \sqrt{x}$ for a 2D system, as $\sqrt{x}$ increases only from 0.4 to 0.5. For x=0.50, the Fermi level has moved into additional bands and the values of the plasma frequency cannot be estimated. The constancy of the values of $\Omega_{p,zz}$ is consistent with the interlayer spacings which do not vary much with the Li content. They will however decrease drastically when large organic molecules are intercalated with the Li, separating the layers considerably and increasing T_c in the process. The Li intercalation appears to enhance hopping along the c axis. For the undoped compound with an interlayer distance of 9.22 Å (with electrons added to simulate the desired doping level) the zz values can drop by an order of magnitude or more:

$$x = 0.16 \quad \Omega_{p,xx} = 2.41, \quad \Omega_{pl,zz} = 0.03 \quad (5)$$

$$x = 0.25 \quad \Omega_{p,xx} = 2.91, \quad \Omega_{pl,zz} = 0.06 \quad (6)$$

B. Dielectric Tensor

Fig. 6 shows the calculated dependence of the real and imaginary part of both components of the dielectric function for the pristine compound as well as for Li_xZrNCl (x= 0.16, 0.25, and 0.50). For undoped ZrNCl the experimental value[47] of the static dielectric constant is $\epsilon_{1,xx}$=5. From the calculated electronic structure we obtain an almost identical value. The dielectric function is featureless until the energy reaches the gap. Above the onset transitions from N 2p valence bands to Zr 3d conduction bands give rise to structure. Structures appear in $\epsilon_{1,xx}$ and $\epsilon_{2,xx}$ at energies in agreement with structures seen in reflectivity measurements (see more discussion below). In $\epsilon_{1,zz}$ and $\epsilon_{2,zz}$ the response is similar with structure appearing at higher energies (above 3.5 eV).

As mentioned above, for $x>$ 0, we focus on $\epsilon(\omega)$ obtained from VCA calculations in which electrons are removed from $Li_{0.5}ZrNCl$ (shown in Fig. 6). In every case the optical spectrum can be divided in two regions: a lower energy range where peaks appear at 1-2 eV linked to interband transitions within the conduction bands occupied by doped-in carriers, and a higher energy range from 3 eV onwards that includes valence-conduction transitions.

In-plane polarization. Superconductivity in this system is clearly associated with the 2D Zr-N bilayer alone as discussed in the Introduction, so we discuss first the xx component. The contribution from doped carriers appears in the 0.7-1.4 eV region, where there is mild interband structure in $\epsilon_{2,xx}$ for x=0.16 and 0.25. For x=0.50, a dramatic change arises due to new interband transitions from the in-plane $d_{x^2-y^2}, d_{xy}$ states to orbitals with more out-of-plane character. The changes in both ϵ_2 and ϵ_1 are dramatic. However, with no noticeable change in superconductivity in this region of doping x, we conclude there is no impact of this change on superconductivity. Doping does not make any significant change in the spectrum above 3 eV as shown in Fig. 6: the changes at higher energy are more regular and understandable from the different level of band filling.

Perpendicular polarization. The strong anisotropy – difference between ϵ_{xx} and ϵ_{zz} – reflects the strong dependence on the momentum matrix elements on the orbitals that are involved. In $\epsilon_{2,zz}$ a peak at 1 eV for x=0.16 shifts towards higher energies with increasing x. At x=0.50 additional strong weight appears in the 2-3 eV range. There is an accompanying change in the structures observed in $\epsilon_{1,zz}$. These alter somewhat the crossings $\epsilon_{1,zz} = 0$ and affect the loss function, which we return to below. The region above 3 eV is altered from its behavior at x=0 but without any evident importance.

C. Reflectivity spectrum

Iwasa *et al.* reported optical reflectivity measurements on Li_xZrNCl,[47] for $x = 0$ and 0.37 with the polarization parallel to the ZrN planes. We have evaluated the reflectivity from the surface boundary condition expression and compared it with the available experimental results.

$$R_{\alpha\alpha} = \left| \frac{\sqrt{\epsilon_{\alpha\alpha}} - 1}{\sqrt{\epsilon_{\alpha\alpha}} + 1} \right|^2 \quad (7)$$

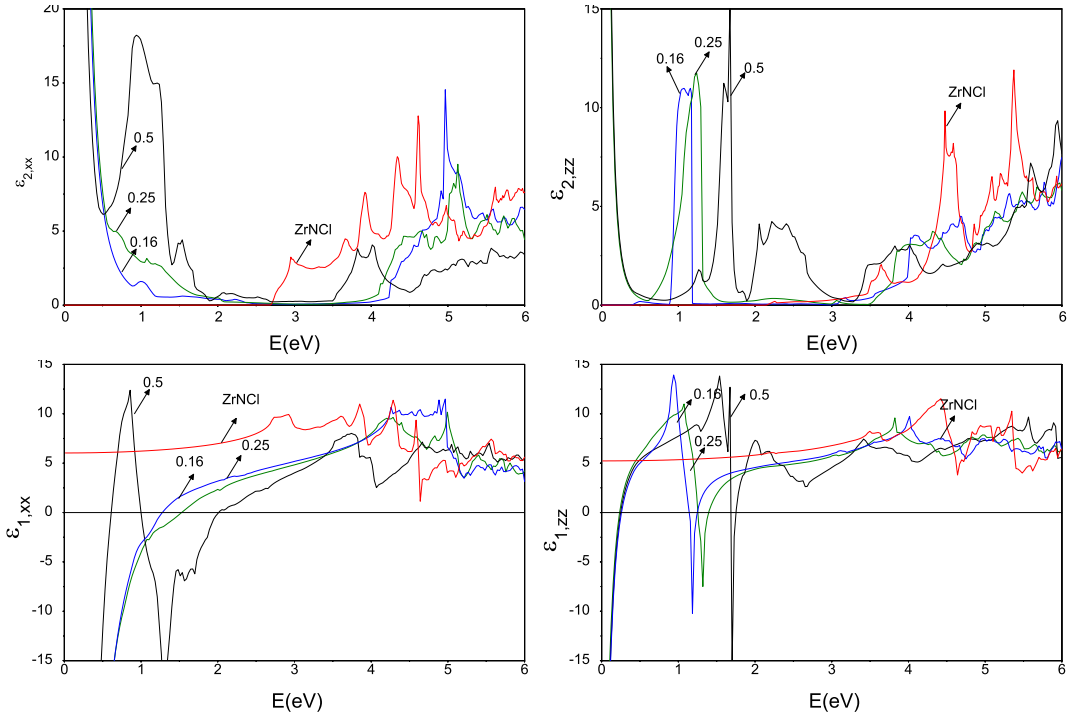

FIG. 6: Comparison of the real ($\epsilon_1(\omega)$, bottom panels) and imaginary ($\epsilon_2(\omega)$, top panels) parts of the dielectric function, for pristine ZrNCl and for Li_xZrNCl (x= 0.16, 0.25 and 0.50).

In experiments, for the insulating compound, the reflectivity decreases slowly with decreasing photon energy in the energy region 0.1-3 eV reflecting its band insulator nature. Prominent peaks appear above 3 eV due to N $2p$ – Zr $4d$ interband transitions with characteristic structures at 3.7, 5.0 and 5.7 eV. In the infrared region below 0.1 eV three peak structures due to the optical phonon modes appear. According to lattice dynamics calculations[52] four IR-active phonon modes have been proposed (20, 33, and 65 meV) – two A modes (displacements along the c-axis) and two E modes (along the ab plane).

Fig.7 shows the optical reflectivity spectra (for both in plane and perpendicular component) of Li_xZrNCl calculated for our chosen doping level.

The behavior for xx polarization is in agreement with the experiment reported by Iwasa *et al.* for the undoped and doped compounds.[47] For the insulating compound, the reflectivity shows the similar behavior for both polarizations, with interband transitions appearing in R_{zz} at higher energy (∼4 eV) than in R_{xx} (∼3 eV) due to matrix element effects, consistent with the description of $\epsilon(\omega)$.

For the doped compounds the Drude-like plasma edge appears upon doping (Fig. 7) as expected for a metal. Metallic reflection already appears below 1 eV for x= 0.16. As the Li doping level is increased,

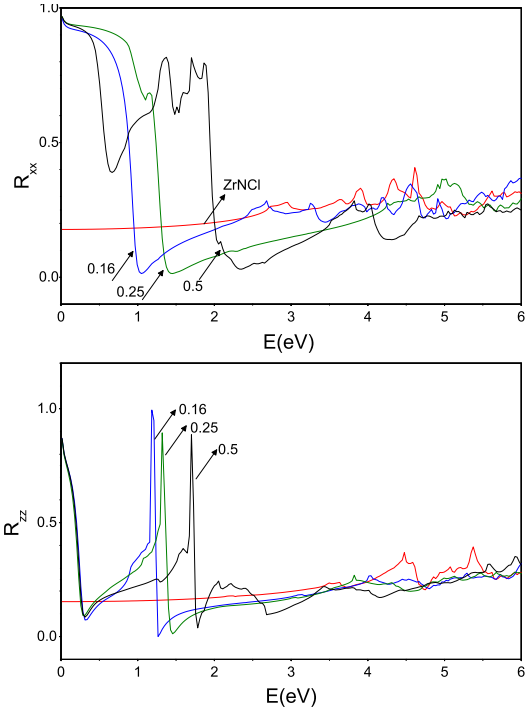

FIG. 7: Doping evolution of the in plane and out of plane components of the optical reflectivity for Li_xZrNCl (x = 0.16, 0.25 and 0.50). The curve for the pristine compound is also shown.

the plasma edge in the reflectivity spectrum shifts towards higher energies for the xx component. The reflectivity edge is sharpened for lower doping levels and the reflectivity below the edge rapidly increases. The behavior is again different at the higher doping level studied due to the above mentioned additional interband transitions from the in-plane to the out of plane orbitals.

For R_{zz} another plasma edge appears at around 0.2 eV being independent of doping level (in this range). We discuss in the following subsection that this invariance is because this edge is purely intraband-derived (whereas that in xx polarization is affected by interband transitions) and the corresponding Drude plasma energies do not vary with doping level. R_{zz} contains similar structure in the 1-2 eV range but it is much sharper and also shifted towards higher energies as the doping level is increased.

The behavior found for Li_xZrNCl can be contrasted with what is observed in systems such as cuprates or Fe-pnictides where also the accumulated data on the normal-state properties seem anomalous in many aspects suggesting an unconventional metallic state is developed. The proximity to a magnetic ground state Fe-pnictides and cuprates makes difficult the direct comparison with non-magnetic $A_x\mathcal{T}$NCl superconductors in any case.

For undoped insulating La_2CuO_4[53,54], with a charge-transfer energy gap of about 2 eV, the spectrum at low energies is very anisotropic and dominated by excitations in the CuO_2 plane with an edge in the xx spectrum appearing at 1 eV indicating the metallic state along CuO2 planes. In the zz reflectivity no structure corresponding to the 1 eV edge is found. In Li_xZrNCl this is not the case as we have seen in the previous description. When substituting La by Sr ($La_{2-x}Sr_xCuO_4$), the spectrum for the polarization perpendicular to the planes does not change substantially in contrast Li_xZrNCl: it is still featureless (typical of an insulator) in the low energy region with the optical phonons dominating even for superconducting compositions. However, drastic changes happen in the spectrum with polarization parallel to the planes where an edge in the reflectivity appears. It is not of the usual Drude type but composed of two contributions: a Drude-like narrow one peaked at ω=0 and a broad continuum centered in the mid-infrared region. The plasma edge in the reflectivity spectrum stays at almost the same position owing to the formation of an in-gap state in the charge transfer gap with doping and is not shifted as the doping level varies as happens in Li_xZrNCl.[53–55]

Infrared reflectivity measurements on several 122 Fe-pnictides[56] also revealed complex features in the xx component of the reflectivity with two electronic subsystems existing. The one gapped due to the spin-density-wave transition in the parent materials such as $Eu(Fe)_2As_2$ is responsible for superconductivity in the doped compounds such as $Ba(Fe_{0.92}Co_{0.08})_2As_2$, $Ba(Fe_{0.95}Ni_{0.08})_2As_2$. The second subsystem gives rise to incoherent background, present in all 122 compounds, which is basically temperature independent but affected by the superconducting transition.

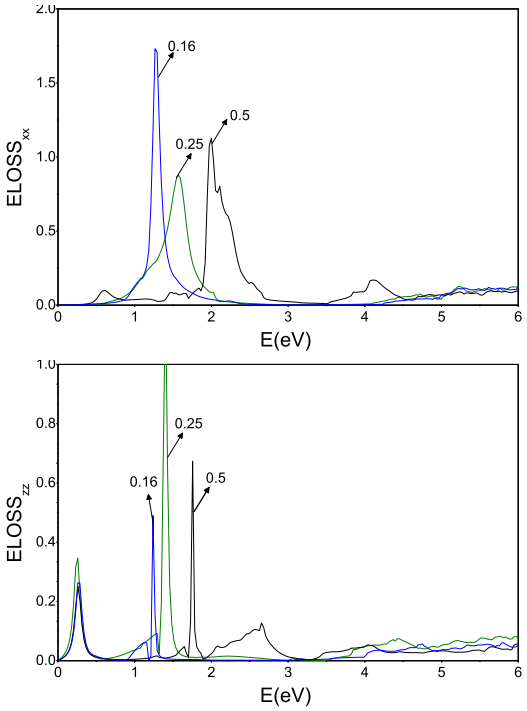

FIG. 8: Doping evolution of the in plane (above) and out of plane (below) components of the energy loss function of Li_xZrNCl ($x = 0.16, 0.25$ and 0.50). Note the decrease in intensity (smaller and narrower peaks) of the plasmon for out of plane polarization.

D. Energy loss spectrum

The energy loss function

$$L_{\alpha\alpha}(\omega) = -\mathrm{Im}\epsilon^{-1}_{\alpha\alpha}(\omega) = \frac{\epsilon_{2,\alpha\alpha}(\omega)}{\epsilon^2_{2,\alpha\alpha}(\omega) + \epsilon^2_{1,\alpha\alpha}(\omega)} \quad (8)$$

is a characteristic response function that can be measured directly, and provides the spectrum energy loss processes. A primary interest is in the collective plasmon peaks and how much they are broadened by interband processes, and the interband losses themselves. Peaks occur where ϵ_2 is small and ϵ_1 passes through zero. Or returning to the reflectivity spectra, the appearance of a reflectivity edge indicates

the presence of a peak in the loss function.

In an ideal 2D interacting electron gas, the plasmon behaves as $\omega_p(q) \propto \sqrt{q}$, hence giving no contribution at q=0. Doped ZrNCl however comprises a periodic superlattice of 2D layers, and in such multilayer systems the long range of the Coulomb interaction (across layers, independent of any electronic hopping) pushes the q=0 plasmon to finite frequency[57] followed by a spectrum at higher frequencies.

The RPA results for $L(\omega)$ for Li_xZrNCl are displayed in Fig. 8. The in-plane (xx) spectrum is dominated by rather well defined plasmon peaks centered at 1.2, 1.5, and 2.0 eV for x=0.16, 0.25, 0.50 respectively. The x=0.50 spectrum is again not quite as simple as those for smaller x, containing a small peak at 0.7 eV and continuing energy loss out to the main peak, and a further structure around 4 eV.

The perpendicular (zz) loss function is different, partly reflecting the large impact of matrix elements that depend strongly on the directionality of the orbitals that are involved in the transition, and also representing different physics. The main plasmon peaks lie at 1.2, 1.5, and 1.8 eV respectively, all lying at roughly the same energy as for xx polarization. They are however much narrower, with full widths at half maximum of 0.1 eV or less. In addition, for each level of doping there is a low energy loss peak around 0.2 eV with larger width. This peak arises from the plasma edge linked to intraband transitions appearing at the same energy in R_{zz}. The highest doping level x=0.5 shows additional interband losses in the 2-3 eV region arising from occupation of the narrower 2nd and 3rd Zr 4d bands.

VI. DISCUSSION

We have studied the q=0 dielectric response of insulating and doped ZrNCl in connection with its impressive superconductivity of uncertain origin. Screening in a layered electron gas as a possible origin of pairing has considerable history. The work by Bill *et al.* was discussed in the Introduction, and Pashitskii and Pentegov[29] have elaborated on some aspects of the plasmon mechanism of pairing. For the layered homogeneous electron gas, the plasmon at $\vec{q} \rightarrow 0$ lies at

$$\omega_p^2 = 4\pi e^2 \frac{n/c}{m^* \epsilon_\infty} \qquad (9)$$
$$\omega_p \approx 2.7\sqrt{x}\ eV$$

for parameters appropriate to ZrNCl: m^*=0.6, ϵ_∞=5, c=10Å. Here n is the 2D density of carriers per unit area. The values are 1.1 eV, 1.4 eV, and 1.9 eV for x=0.16, 0.25, 0.50 respectively, which are very similar to our computed values 1.2 eV, 1.5 eV, and 2.0 eV that can be seen in Fig. 8. Note that if the cell spacing c is doubled ω_p decreases by $2^{1/2}$; such an increase is observed to result in an increase T_c by 30%. At this spacing and at the critical concentration x_{cr}=0.06, $\omega_p \sim 0.5$ eV.

Formulation of a realistic superconducting gap equation and hence T_c is a daunting task. Atwal and Ashcroft built a model appropriate for polarization waves of semicore electrons and estimated that T_c of a few tens of kelvins could result.[58] The model of Bill *et al.*[28] was adapted to doped HfNCl, concluding that T_c = 25K could readily be obtained with realistic parameters. With their version of approximating the plasmon pairing kernel, Pashitskii and Pentegov[29] found a very strong dependence on carrier concentration (unlike observations in the metal nitridochloride system) and could reach $T_c \sim$ 150K.

Without building specific models and in the context of increasing T_c in several classes of one-, two-, and three-layered cuprates, Leggett focused on the Coulomb interaction energy, first within an isolated two-dimensional electron gas, and then on the interaction between such layers. He argued[59] that the gain in Coulomb interaction energy upon entering the superconducting state is greater for several layers versus a single layer. His approach also predicted a majority of the effect to be from small-q screening (long distance interaction).

What remains in the dynamics of these doped metal nitridochlorides (beyond the full q-dependence of $\epsilon(q,\omega)$) is the background of vibrating, highly charged ions in materials like lightly doped ZrNCl. This dynamics is implicated in the very bad metal behavior of resistivity discussed in the Introduction. Born effective charges have been reported for ZrNCl,[12] with the Zr^{4+} having a BEC of +2.7 in-plane, N^{3-} of -2.0 and Cl^{1-} of -0.7. A significant anisotropy is found (the out of plane BEC are 1.1, -0.7 and -0.5 for Zr^{4+}, N^{3-}, and Cl1−, respectively) due to the layered structure of the system. For a similar layered ionic insulator $BaHfN_2$, the Hf^{4+} ion has a BEC of +4.5 in-plane, with N^{3-} values up to -4.5 and Ba^{2+} a BEC around +3.[60]

There will be strong Coulomb coupling between these vibrating ions and the low density two dimensional electron gas, possibly giving rise to polaronic behavior near or below the critical doping level of 0.06. There is a large literature on modeling polarons and on bipolaronic mechanisms of pairing. However, specific treatments are needed: there are many cases of doped layered ionic insulators, but only this one class of excellent superconductors with $T_c \sim$ 15-26K.

VII. SUMMARY

We have studied the q=0 dielectric response of insulating and Li-doped ZrNCl in connection with its impressive superconductivity of unknown origin. We have revisited the electronic structure of Li_xZrNCl, establishing that the differences between rigid band modeling and virtual crystal treatment are small, and comparing the results also with actual lithium doping using supercells. We have analyzed the dependence of the dielectric response with frequency and doping level, reproducing the experimental static dielectric constant ϵ_∞=5 extremely well. In the reflectivity spectra the appearance of a Drude plasma edge demonstrates the transition from a band insulator to a metal upon Li-intercalation. In the energy loss function, the main plasmon peaks appear where the electron gas model suggests they should, in the range 1.2-2.0 eV for x varying from 0.16 to 0.50. The variations upon changing the doping level found in our calculations of the reflectivity and energy loss function are not correlated with the observed experimental (non)variation of $T_c(x)$, providing useful data in the search for the pairing mechanism in this class of superconductors. Specifically, pairing based on straightforward electronic overscreening is not supported by our results.

VIII. ACKNOWLEDGMENTS

The authors have benefited from discussions with F. Gygi, D. J. Scalapino, M. L. Cohen, P. C. Canfield, and M. Calandra. This project was supported by the NSF Grant DMR-1207622.

[1] V. L. Ginzburg and D. A. Kirzhnits, Sov. Phys. JETP **19**, 269 (1964).
[2] V. L. Ginzburg and D. A. Kirzhnits, *High-Temperature Superconductivity* (Consultant Bureau Plenum, 1982).
[3] W. E. Pickett, Physica B **296**, 112 (2001).
[4] S. Yamanaka, K. Hotehama, and H. Kawaji, Nature **392**, 580 (1998).
[5] S. Yamanaka, T. Yasunaga, K. Yamaguchia, and M. Tagawaa, J. Mater. Chem. **19**, 2573 (2009).
[6] S. Yamanaka, H. Kawaji, K. Hotehama, and M. Ohashi, Adv. Mater. **9**, 771 (1996).
[7] Y. Kasahara, T. Kishiume, K. Kobayashi, Y. Taguchi, and Y. Iwasa, Phys. Rev. B **82**, 054504 (2010).
[8] S. Zhang, M. Tanaka, H. Zhu, and S. Yamanaka, Supercond. Sci. Technol. **26**, 085015 (2013).
[9] S. Zhang, M. Tanaka, and S. Yamanaka, Phys. Rev. B **86**, 024516 (2012).
[10] Y. Taguchi, A. Kitora, and Y. Iwasa, Phys. Rev. Lett. **97**, 107001 (2006).
[11] Y. Taguchi, A. Kitora, M. Hisakabe, and Y. Iwasa, Physica B **383**, 67 (2006).
[12] R. Heid and K.-P. Bohnen, Phys. Rev. B **72**, 134527 (2005).
[13] R. Weht, A. Filipetti, and W. E. Pickett, Europhys. Lett. **48**, 320 (1999).
[14] T. Takano, A. Kitora, Y. Taguchi, and Y. Iwasa, Phys. Rev. B **77**, 104518 (2008).
[15] R. Akashi, K. Nakamura, R. Arita, and M. Imada, Phys. Rev. B **86**, 054513 (2012).
[16] H. Kotegawa, S. Oshiro, Y. Shimizu, H. Tou, Y. Kasahara, T. Kishiume, Y. Taguchi, and Y. Iwasa, arXiv:1407.3031 (2014).
[17] Y. Kasahara, T. Kishiume, T. Takano, K. Kobayashi, E. Matsuoka, H. Onodera, K. Kuroki, Y. Taguchi, and Y. Iwasa, Phys. Rev. Lett. **103**, 077004 (2009).
[18] K. Kuroki, Phys. Rev. B **81**, 104502 (2010).
[19] R. Jaramillo, S. D. Ha, D. M. Silevitch, and S. Ramanathan, Nat. Phys. **10**, 304 (2014).
[20] Z. P. Yin, A. Kutepov, and G. Kotliar, Phys. Rev. X **3**, 021011 (2013).
[21] H. Tou, Y. Maniwa, and S. Yamanaka, Phys. Rev. B **67**, 100509 (2003).
[22] Y. Taguchi, T. Kawabata, T. Takano, A. Kitora, K. Kato, M. Takata, and Y. Iwasa, Phys. Rev. B **76**, 064508 (2007).
[23] M. Lüders, M. A. L. Marques, N. N. Lathiotakis, A. Floris, G. Profeta, L. Fast, A. Continenza, S. Massidda, and E. K. U. Gross, Phys. Rev. B **72**, 024545 (2005).
[24] A. Floris, G. Profeta, N. N. Lathiotakis, M. Lüders, M. A. L. Marques, C. Franchini, E. K. U. Gross, A. Continenza, and S. Massidda, Phys. Rev. Lett. **94**, 037004 (2005).
[25] A. Sanna, G. Profeta, A. Floris, A. Marini, E. K. U. Gross, and S. Massidda, Phys. Rev. B **75**, 020511(R) (2007).
[26] G. Profeta, C. Franchini, N. N. Lathiotakis, A. Floris, A. Sanna, M. A. L. Marques, M. Lüders, S. Massidda, E. K. U. Gross, and A. Continenza, Phys. Rev. Lett. **96**, 047003 (2006).
[27] A. Bill, H. Morawitz, and V. Z. Kresin, Phys. Rev. B **66**, 100501(R) (2002).
[28] A. Bill, H. Morawitz, and V. Z. Kresin, Phys. Rev. B **68**, 144519 (2003).
[29] E. A. Pashitskii and V. I. Pentegov, Low Temp. Phys. **34**, 113 (2008).
[30] X. Chena, T. Koiwasakiba, and S. Yamanaka, J. Solid State Chem. **159**, 80 (2001).
[31] X. Chen, L. Zhu, and S. Yamanaka, J. Solid State Chem. **169**, 149 (2002).
[32] R. Juzatr and H. Friedrichsen, Z. Anorg. Allg. Chem. **332**, 173 (1964).
[33] S. Shamoto, T. Kato, Y. Ono, Y. Miyazaki, K. Ohoyama, M. Ohashi, Y. Yamaguchi, and T. Kajitani, Physica C **306**, 7 (1998).

[34] P. Blaha, K. Schwarz, G. K. H. Madsen, D. Kvasnicka, and J. Luitz, *WIEN2k, An Augmented Plane Wave Plus Local Orbitals Program for Calculating Crystal Properties. ISBN 3-9501031-1-2*, Vienna University of Technology, Austria (2001).
[35] K. Schwarz and P. Blaha, Comp. Mat. Sci. **28**, 259 (2003).
[36] P. Hohenberg and W. Kohn, Phys. Rev. **136**, B864 (1964).
[37] R. O. Jones and O. Gunnarsson, Rev. Mod. Phys. **61**, 689 (1989).
[38] E. Sjöstedt, L. Nördstrom, and D. J. Singh, Solid State Commun. **114**, 15 (2000).
[39] J. P. Perdew, K. Burke, and M. Ernzerhof, Phys. Rev. Lett. **77**, 3865 (1996).
[40] C. Ambrosch-Draxl and J. Sofo, Comp. Phys. Commun. **175**, 1 (2006).
[41] A. Kokalj, J. Mol. Graphics Modell. **17**, 176 (1999).
[42] T. Yokoya, T. Takeuchi, S. Tsuda, T. Kiss, T. Higuchi, S. Shin, K. Iizawa, S. Shamoto, T. Kajitani, and T. Takahashi, Phys. Rev. B **70**, 193103 (2004).
[43] C. Felser and R. Seshadri, J. Mater. Chem. **9**, 459 (1999).
[44] Q. Yin, E. R. Ylvisaker, and W. E. Pickett, Phys. Rev. B **83**, 014509 (2011).
[45] Y. Taguchi, M. Hisakabe, and Y. Iwasa, Phys. Rev. Lett. **94**, 217002 (2005).
[46] E. R. Ylvisaker and W. E. Pickett, EPL **101**, 57006 (2013).
[47] T. Takano, A. Kitora, Y. Taguchi, and Y. Iwasa, J. Phys. Chem. Solids **69**, 3089 (2009).
[48] T. Yokoya, Y. Ishiwata, S. Shin, S. Shamoto, K. Iizawa, T. Kajitani, I. Hase, and T. Takahashi, Phys. Rev. B **64**, 153107 (2001).
[49] T. Yokoya, T. Takeuchi, S. Tsuda, T. Kiss, T. Higuchi, S. Shin, K. Iizawa, S. Shamoto, T. Kajitani, and T. Takahashi, Phys. Rev. B **70**, 193103 (2004).
[50] N. W. Ashcroft and N. D. Mermin, *Solid State Physics* (Saunders College Publishing, Fort Worth TX, 1976).
[51] J. Lindhard, Dan. Mat. Fys. Medd. **28**, No. 8 (1954).
[52] P. Adelmann, B. Renker, H. Schober, M. Braden, and F. Fernandez-Diaz, J. Low Temp. Phys **117**, 449 (1999).
[53] S. Uchida, T. Ido, H. Takagi, T. Arima, Y. Tokura, and S. Tajima, Phys. Rev. B **43**, 7942 (1991).
[54] D. N. Basov, H. A. Mook, B. Dabrowski, and T. Timusk, Phys. Rev. B **52**, R13141 (1995).
[55] Y. H. Kim and P. H. Hor, J. Phys.: Condens. Matter **25**, 355702 (2013).
[56] D. Wu, N. Barisic, P. K. A. Faridian, B. Gorshunov, N. Drichko, L. J. Li, X. Lin, G. H. Cao, Z. A. Xu, N. L. Wang, et al., Phys. Rev. B **81**, 100512(R) (2010).
[57] J. K. Jain and P. B. Allen, Phys. Rev. Lett. **54**, 2437 (1985).
[58] G. S. Atwal and N. W. Ashcroft, Phys. Rev. B **70**, 104513 (2004).
[59] A. J. Leggett, Phys. Rev. Lett. **83**, 392 (1999).
[60] A. Kaur, E. R. Ylvisaker, Y. Li, G. Galli, and W. E. Pickett, Phys. Rev. B **82**, 155125 (2010).